Electronic Supplementary Material (ESI) for Inorganic Chemistry Frontiers.

SUPPORTING INFORMATION

Spin transition and symmetry-breaking in new mononuclear Fe^{II} tren-complexes with up to 38 K hysteresis around room temperature

M. Seredyuk, K. Znovjyak, F.-J. Valverde-Muñoz, M. C. Muñoz, I. O. Fritsky, V. M. Amirkhanov, and J. A. Real

SYNTHESIS AND PHYSICAL CHARACTERIZATION

Physical measurements. Variable-temperature **magnetic susceptibility data** (15-20 mg) were recorded on melted samples using a Quantum Design MPMS2 SQUID susceptometer operating at 1 T magnet. The LIESST experiments were performed at 10 K in a commercial sample holder (Quantum Design Fiber Optic Sample Holder), wherein a quartz bucket containing *ca*. 1 mg of microcrystals was held against the end of a quartz fiber coupled with a red laser (633 nm, 10 mW cm^{-1}). The raw data were corrected for a paramagnetic background arising from the sample holder. The resulting magnetic signal was calibrated by scaling to match values with those of bulk sample. **DSC** measurements were performed on a Mettler Toledo TGA/SDTA 821e under a nitrogen atmosphere with a rate of 10 K min^{-1}. The raw data were analyzed with the Netzsch Proteus software with an overall accuracy of 0.2 K in the temperature and 2 % in the heat flow. **Elemental CHN analysis** was performed after combustion at 850 °C using IR detection and gravimetry by means of a Perkin–Elmer 2400 series II device. **X-ray powder diffraction** measurements were performed on a PANalytical Empyrean X-ray powder diffractometer (monochromatic Cu K_α radiation) equipped with open flow cryostat. The measurements were collected at 4 K intervals on heating and 10 K intervals on cooling. Each plot is a superposition of three scans collected at the rate 5.6 ° min^{-1}. **^{57}Fe Mössbauer spectra** were recorded in transmission geometry on a conventional spectrometer operating in constant-acceleration mode with ^{57}Co/Rh source kept at RT. The samples were sealed in a Plexiglass sample holder and mounted in a nitrogen-bath cryostat. The spectroscopic evaluations were performed with the assumption of Lorentzian line-shapes by using the Recoil 1.05 Mössbauer Analysis Software (Dr. E. Lagarec). All isomeric shifts are given relative to the α-Fe at RT.

Single crystal X-ray diffraction. Single-crystal X-ray data of **1-BF_4** were collected on a single crystal diffractometer using graphite mono-chromated MoK_α radiation (λ = 0.71073 Å). A multi-scan absorption correction was performed. The structures were solved by direct methods using SHELXS-2014 and refined by full-matrix least squares on F^2 using SHELXL-2014.[1] Non-hydrogen atoms were refined anisotropically and hydrogen atoms were placed in calculated positions refined using idealized geometries (riding model) and assigned fixed isotropic displacement parameters. The

octahedral distortion parameters ζ, Σ, and Θ of the coordination sphere were calculated using program OctaDist 2.6.1.[2] CCDC files 2024798, 2024799 and 2091080 contain the supplementary crystallographic data for this paper. These data can be obtained free of charge from The Cambridge Crystallographic Data Centre via www.ccdc.cam.ac.uk/data_request/cif.

Synthesis of complexes. All chemicals were purchased from commercial suppliers and used without further purification.

The ligand was obtained by condensation 6-fluorpyridine-2-carboxaldehyde (122 mg, 88.8 mmol) and tris(2-aminoethyl)amine (43 mg, 29.6 mmol) in boiling $EtOH_{abs.}$ (5 ml) during 15 min. Subsequent complexation with $Fe(BF_4)_2 \cdot 6H_2O$ (100 mg, 29.6 mmol) or $Fe(ClO_4)_2 \cdot nH_2O$ (112 mg, 29.6 mmol) dissolved in $EtOH_{abs.}$ (5 ml) led to the formation of black drops deposited on the walls and bottom of the reaction vial. Upon standing under mother liquor during approx. two weeks the oils converted into dark crystalline material which was filtered off, washed with ethanol and dried.

1-BF_4. Elemental analysis calcd. (%) for $C_{24}H_{24}B_2F_{11}FeN_7$: C, 41.36; H, 3.47; N, 14.07. Found: C, 41.54; H, 3.52; N, 14.29.

1-ClO_4. Elemental analysis calcd. (%) for $C_{24}H_{24}Cl_2F_3FeN_7O_8$: C, 39.91; H, 3.35; N, 13.58. Found: C, 40.34; H, 3.21; N, 13.39.

Table S1. Crystallographic data for **1-BF_4**.

Temperature	**180 K**	**265 K**	**280 K**
Empirical formula	$C_{48}H_{48}N_{14}B_4F_{22}Fe_2$	$C_{48}H_{48}N_{14}B_4F_{22}Fe_2$	$C_{24}H_{24}N_7B_2F_{11}Fe$
M_r	1393.94	1393.94	696.97
Crystal system	monoclinic	monoclinic	monoclinic
Space group	$P2_1/n$	$P2_1/n$	$P2_1/c$
a (Å)	19.50(2)	19.712(8)	10.785(6)
b (Å)	19.61(3)	19.783(8)	18.859(11)
c (Å)	14.57(2)	14.687(6)	14.369(8)
β (°)	84.95(4)	85.671(11)	93.21(2)
V (Å^3)	5550(12)	5711(4)	2918(3)
Z	4	4	4
D_c (mg cm^{-3})	1.668	1.621	1.587
F(000)	2816	2816	1408
μ (Mo-K_α) (mm^{-1})	0.648	0.630	0.617
No. of total reflections	4167	13076	6372
No. of reflections [$I > 2\sigma(I)$]	3146	3661	3513
R [$I > 2\sigma(I)$]	0.0458	0.094	0.0709
wR [$I > 2\sigma(I)$]	0.1170	0.370	0.1989
S	0.771	0.960	0.929

$R = \Sigma \, ||Fo| - |Fc|| \, / \, \Sigma \, |Fo|$; $wR = [\, \Sigma \, [w(Fo^2 - Fc^2)^2] \, / \, \Sigma \, [w(Fo^2)^2]]^{1/2}$.
$w = 1/[\sigma^2(Fo^2) + (m\,P)^2 + n\,P]$ where $P = (Fo^2 + 2Fc^2)/3$;
m = 0.0871 (**1** (**180 K**)), 0.159 (**1 (265 K)**), 0.1777 (**1** (**280 K**));
n = 47.2666 (**1** (**180 K**)), 0 (**1 (265 K)**), 2.8129 (**1** (**280 K**))

Table S2. Selected bond lengths [Å] and angles [°] for **1-BF_4**.

180 K			
Fe(A)-N1(A)	2.019(7)	Fe(B)-N1(B)	2.024(7)
Fe(A)-N2(A)	1.958(7)	Fe(B)-N2(B)	1.960(7)
Fe(A)-N3(A)	2.017(7)	Fe(B)-N3(B)	2.023(7)
Fe(A)-N4(A)	1.948(7)	Fe(B)-N4(B)	1.956(7)
Fe(A)-N5(A)	2.035(7)	Fe(B)-N5(B)	2.036(7)
Fe(A)-N6(A)	1.969(7)	Fe(B)-N6(B)	1.942(7)
N2(A)-Fe(A)-N1(A)	80.8(3)	N2(B)-Fe(B)-N1(B)	80.7(3)
N1(A)-Fe(A)-N3(A)	97.0(3)	N1(B)-Fe(B)-N3(B)	97.8(3)
N4(A)-Fe(A)-N1(A)	88.8(3)	N4(B)-Fe(B)-N1(B)	87.5(3)
N1(A)-Fe(A)-N5(A)	97.8(3)	N1(B)-Fe(B)-N5(B)	95.2(3)
N2(A)-Fe(A)-N4(A)	95.9(3)	N2(B)-Fe(B)-N4(B)	94.6(3)
N2(A)-Fe(A)-N5(A)	87.1(3)	N2(B)-Fe(B)-N5(B)	86.3(3)
N2(A)-Fe(A)-N6(A)	95.0(3)	N6(B)-Fe(B)-N2(B)	94.8(3)
N4(A)-Fe(A)-N3(A)	80.7(3)	N4(B)-Fe(B)-N3(B)	81.4(3)
N3(A)-Fe(A)-N5(A)	96.4(3)	N3(B)-Fe(B)-N5(B)	97.9(3)
N6(A)-Fe(A)-N3(A)	87.3(3)	N6(B)-Fe(B)-N3(B)	86.9(3)
N4(A)-Fe(A)-N6(A)	92.7(3)	N6(B)-Fe(B)-N4(B)	96.1(3)
N6(A)-Fe(A)-N5(A)	80.8(3)	N6(B)-Fe(B)-N5(B)	81.2(3)

265 K				280 K	
Fe(A)-N1(A)	2.044(8)	Fe(B)-N1(B)	2.094(8)	Fe(1)-N(1)	2.244(5)
Fe(A)-N2(A)	1.984(8)	Fe(B)-N2(B)	2.005(9)	Fe(1)-N(2)	2.105(5)
Fe(A)-N3(A)	2.044(8)	Fe(B)-N3(B)	2.102(8)	Fe(1)-N(3)	2.321(5)
Fe(A)-N4(A)	1.961(8)	Fe(B)-N4(B)	1.974(9)	Fe(1)-N(4)	2.118(5)
Fe(A)-N5(A)	2.077(8)	Fe(B)-N5(B)	2.110(8)	Fe(1)-N(5)	2.289(5)
Fe(A)-N6(A)	1.985(8)	Fe(B)-N6(B)	1.962(9)	Fe(1)-N(6)	2.110(5)
N2(A)-Fe(A)-N1(A)	80.0(3)	N2(B)-Fe(B)-N1(B)	78.9(4)	N(1)-Fe(1)-N(2)	75.3(2)
N3(A)-Fe(A)-N1(A)	96.5(3)	N1(B)-Fe(B)-N3(B)	97.6(3)	N(1)-Fe(1)-N(3)	96.0(2)
N4(A)-Fe(A)-N1(A)	89.1(3)	N4(B)-Fe(B)-N1(B)	87.6(3)	N(1)-Fe(1)-N(4)	87.1(2)
N1(A)-Fe(A)-N5(A)	97.7(3)	N1(B)-Fe(B)-N5(B)	94.3(3)	N(1)-Fe(1)-N(5)	95.2(2)
N4(A)-Fe(A)-N2(A)	96.7(3)	N4(B)-Fe(B)-N2(B)	96.6(4)	N(2)-Fe(1)-N(4)	105.7(2)
N4(A)-Fe(A)-N6(A)	94.1(3)	N2(B)-Fe(B)-N5(B)	85.9(3)	N(2)-Fe(1)-N(5)	87.5(2)
N2(A)-Fe(A)-N5(A)	86.9(3)	N6(B)-Fe(B)-N2(B)	98.4(4)	N(2)-Fe(1)-N(6)	101.0(2)
N2(A)-Fe(A)-N6(A)	96.0(3)	N4(B)-Fe(B)-N3(B)	80.2(3)	N(3)-Fe(1)-N(4)	73.7(2)
N4(A)-Fe(A)-N3(A)	80.5(3)	N3(B)-Fe(B)-N5(B)	97.4(3)	N(3)-Fe(1)-N(5)	93.1(2)
N3(A)-Fe(A)-N5(A)	96.2(3)	N6(B)-Fe(B)-N3(B)	85.4(3)	N(3)-Fe(1)-N(6)	87.5(2)
N6(A)-Fe(A)-N3(A)	87.6(3)	N6(B)-Fe(B)-N4(B)	99.6(3)	N(4)-Fe(1)-N(6)	103.6(2)
N6(A)-Fe(A)-N5(A)	79.3(3)	N6(B)-Fe(B)-N5(B)	78.6(3)	N(5)-Fe(1)-N(6)	74.5(2)

Table S3. Structural and distortion parameters for **1-BF_4** and related compounds.

	T/K		<Fe–N>/Å	*V*/Å^3	Θ[a]	Σ[b]	ζ[c]	CShM (O_h)[d]	CShM (D_{3h})[d]
1-BF_4	180	Fe(A)	1.991(8)	10.310(8)	204.85(3)	69.35(3)	0.195(8)	0.777	15.167
		Fe(B)	1.990(8)	10.296(8)	205.47(3)	72.28(3)	0.225(8)	0.765	15.474
		<Fe>	1.991(8)	10.303(8)	205.16(3)	70.82(3)	0.210(8)	0.771	15.321
	265	Fe(A)	2.016(8)	10.679(8)	219.18(3)	73.65(3)	0.234(8)	0.888	15.129
		Fe(B)	2.041(8)	10.999(8)	250.68(3)	87.33(3)	0.363(8)	1.102	15.185
		<Fe>	2.029(8)	10.839(8)	234.93(3)	80.53(3)	0.298(8)	0.995	15.157
	280		2.198(6)	13.385(6)	334.28(2)	109.07(2)	0.522(6)	1.979	14.950
$\{Fe^{II}[tren(py)_3]\}(ClO_4)_2$[3]	110		1.961(9)	9.892(9)	182.77(3)	61.38(3)	0.074(9)	0.597	15.340
$\{Fe^{II}[tren(6Me\text{-}py)_3]\}$-$(ClO_4)_2$[4]	80		2.015(1)	10.580(1)	231.10(5)	83.81(5)	0.389(1)	1.172	15.223
	330		2.216(2)	13.759(2)	336.62(9)	111.01(9)	0.521(2)	2.083	15.311

[a] $\Theta = \Sigma_1^{24}(|60 - \vartheta_i|)$, ϑ_i is the angle generated by superposition of two opposite faces of the octahedron[5]
[b] $\Sigma = \Sigma_1^{12}(|90 - \varphi_i|)$, φ_i is angle N–Fe–N'[6]
[c] $\zeta = \Sigma_1^{6}(|\text{<Fe–N>} - \text{Fe–N}_i|)$, N_i is one of the six nitrogen atoms forming polyhedron $[FeN_6]$[7]
[d] Continuous shape measure[8]

Table S4. Short intermolecular contacts of **1-BF_4** below the van der Waals radii.

Short contacts at 180 K	Length (Å)
C24A··· F8A	3.051(8)
C13B··· F10A	3.061(8)
C2B··· F9B	3.085(8)
C16A··· F9A (-1/2-*x*,1/2+*y*,1/2-*z*)	3.113(8)
C24B··· F4A	3.116(8)
C4A··· F9B (-1/2-*x*,1/2+*y*,1/2-*z*)	3.118(8)
C12B··· C12B (-*x*,1-*y*,-*z*)	3.126(8)
C2A··· F4A (-1/2+*x*,1.5-*y*,1/2+*z*)	3.127(8)
C14A··· F10B (-1/2-*x*,1/2+*y*,1/2-*z*)	3.144(8)
C16A··· F5A	3.161(8)
C14A··· C4B (-1/2-*x*,1/2+*y*,1.5-*z*)	3.323(8)
C17A··· C13B	3.399(8)

Short contacts at 265 K	Length (Å)
C4A···F9B (-1/2-*x*,1/2+*y*,1/2-*z*)	3.084(8)
C24A···F8A	3.093(8)
C2B···F9B	3.121(8)
C13B···F10A	3.126(8)
C16A···F9A (-1/2-*x*,1/2+*y*,1/2-*z*)	3.135(8)
C2A···F4A	3.140(8)
C12B···C12B (-*x*,1-*y*,-*z*)	3.143(8)
C16A···F6A (1/2+*x*,1.5-*y*,-1/2+*z*)	3.162(8)
C14A···C4B (-1/2-*x*,1/2+*y*,1.5-*z*)	3.362(8)

Short contacts at 280 K, HS	Length (Å)
C12··· F8	3.078(6)
C16···F7	3.115(6)
C1···F5	3.119(6)
C19···F11(1-*x*,-1/2+*y*,1.5-*z*)	3.155(6)
C2···C2 (1-*x*,1-*y*,-*z*)	3.176(6)

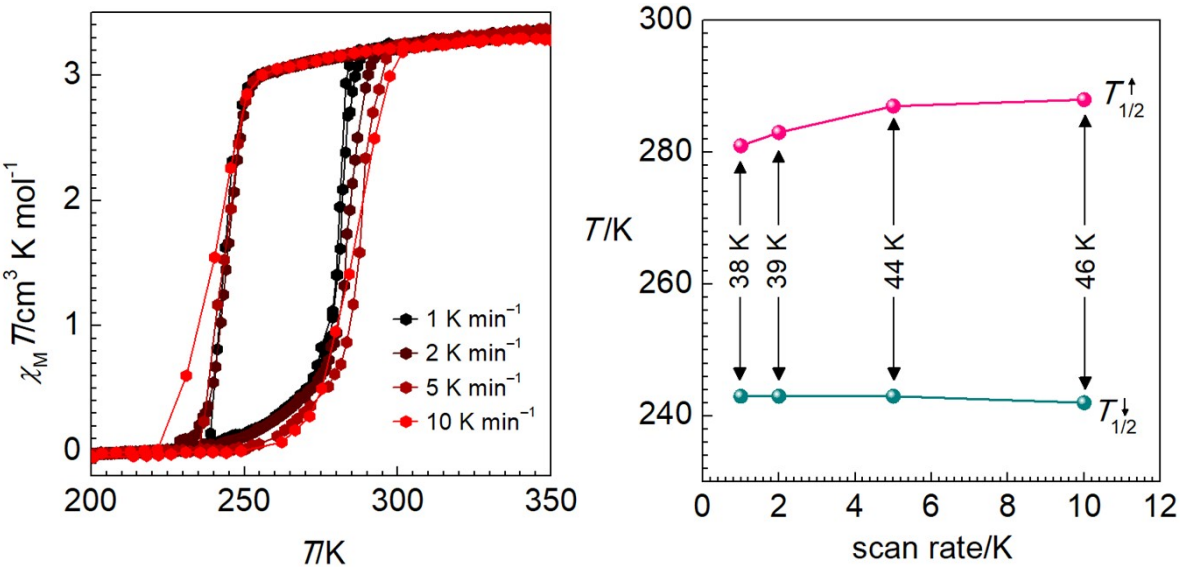

Figure S1. (a) Plot $\chi_M T$ vs T for **1-BF₄** at different scan rates; (b) Dependence of the $T_{1/2}^{\uparrow/\downarrow}$ and derived ΔT_h on the scan rate.

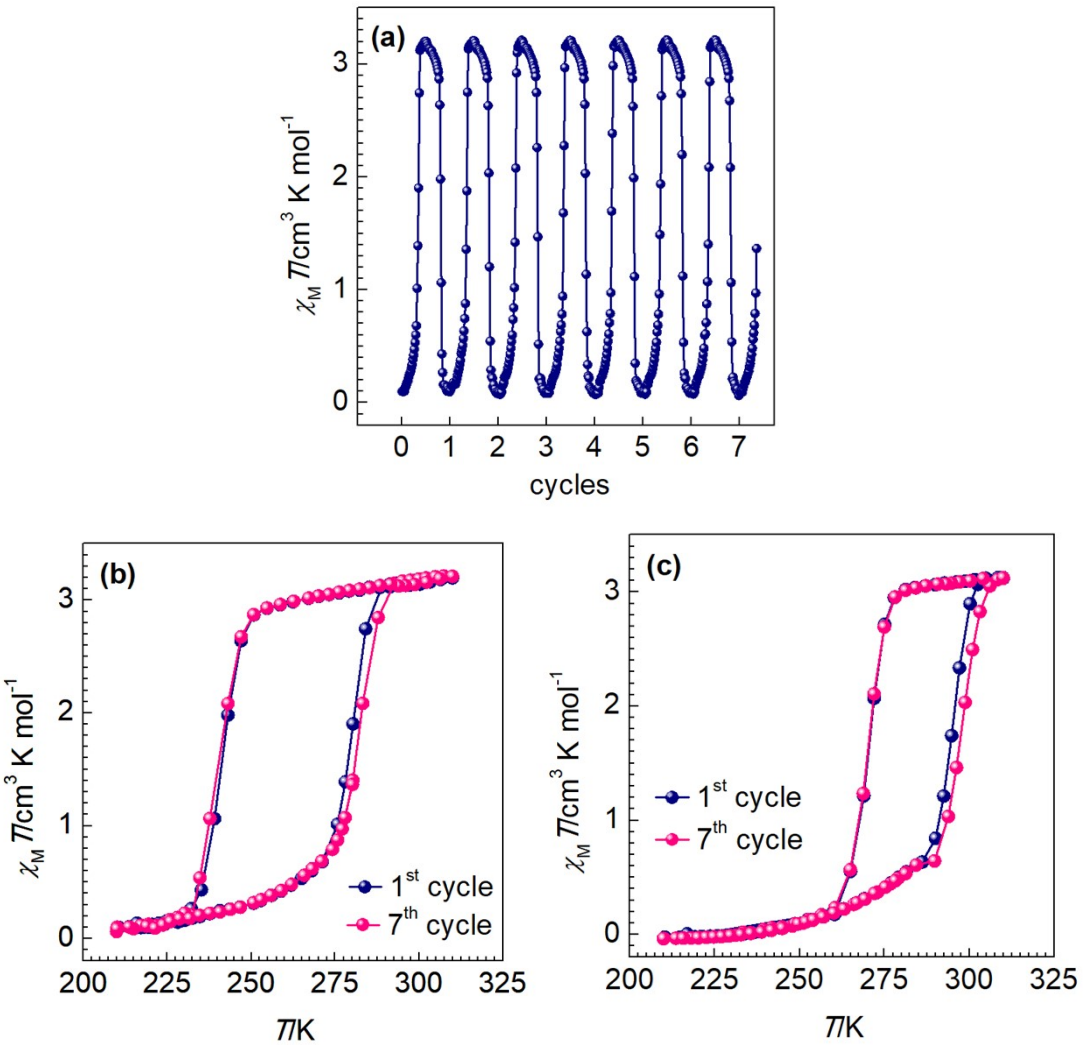

Figure S2. (a) Thermal cycling of **1-BF₄**. Overlay of the cycles for **1-BF₄** (b) and for **1-ClO₄** (c).

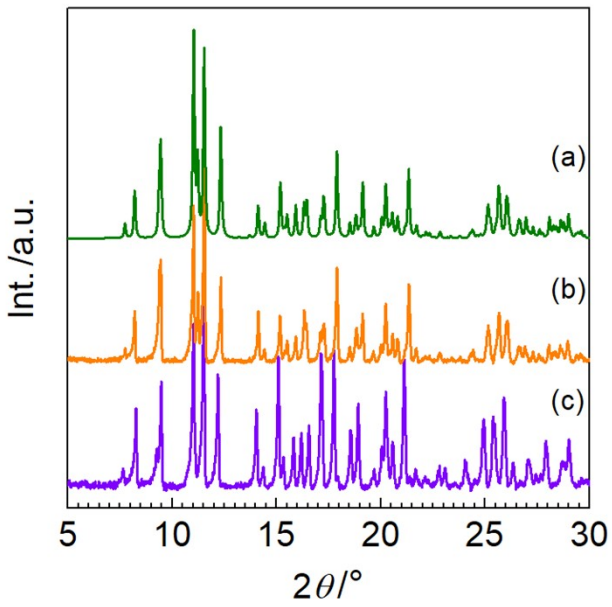

Figure S3. Comparison of theoretically calculated XRD profile of **1-BF_4** at 280 K (a) with the experimental profiles of **1-BF_4** (b) and **1-ClO_4** (c) at room temperature.

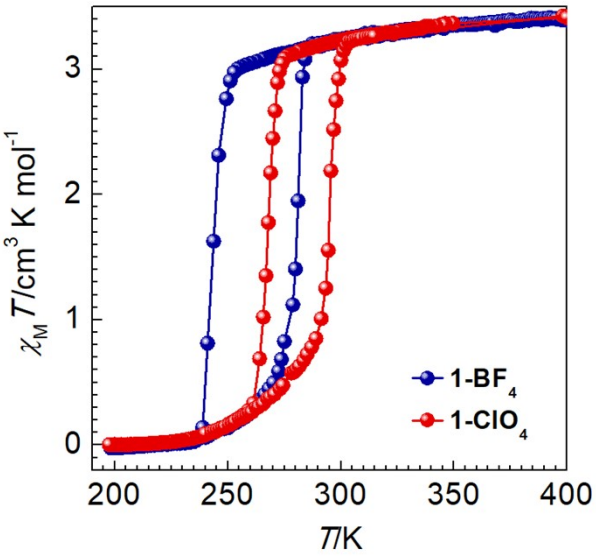

Figure S4. Overlaying magnetic curves mismatch only in the position of the hysteretic loops.

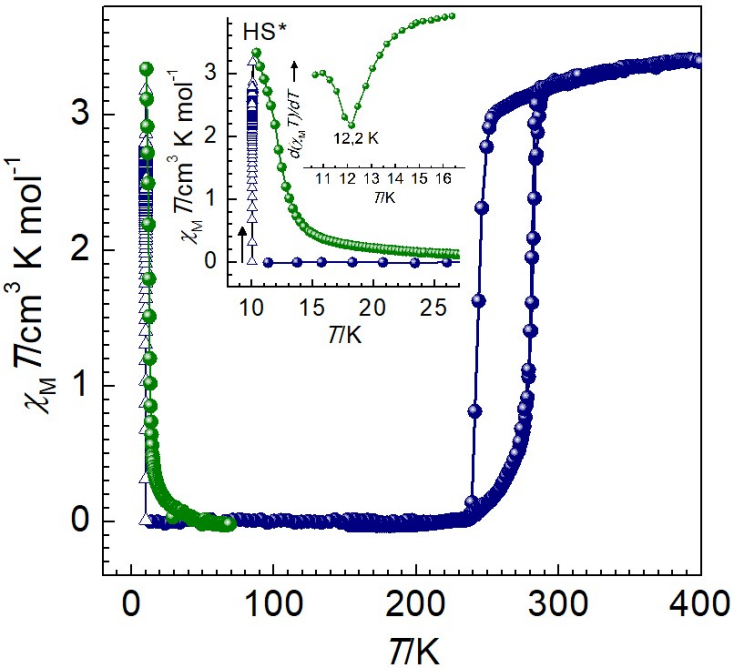

Figure S5. The LIESST experiment for **1-BF$_4$** at 0.3 K min^{-1}.

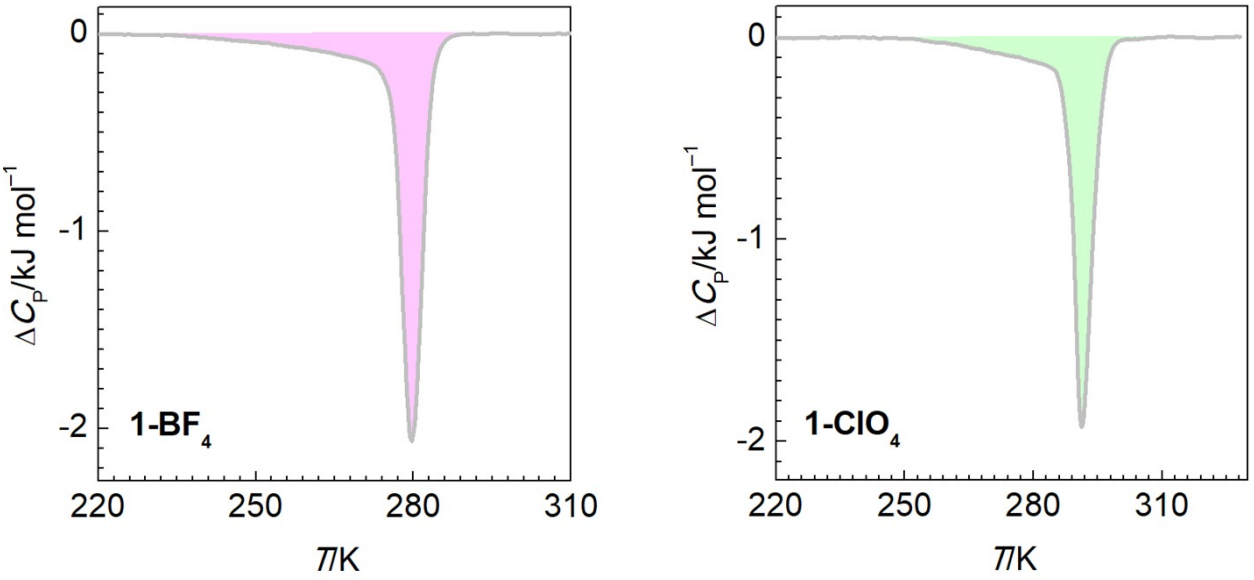

Figure S6. "Gradual" and "steep" parts in the endothermic peak of **1-BF$_4$** and **1-ClO$_4$** on the heating run.

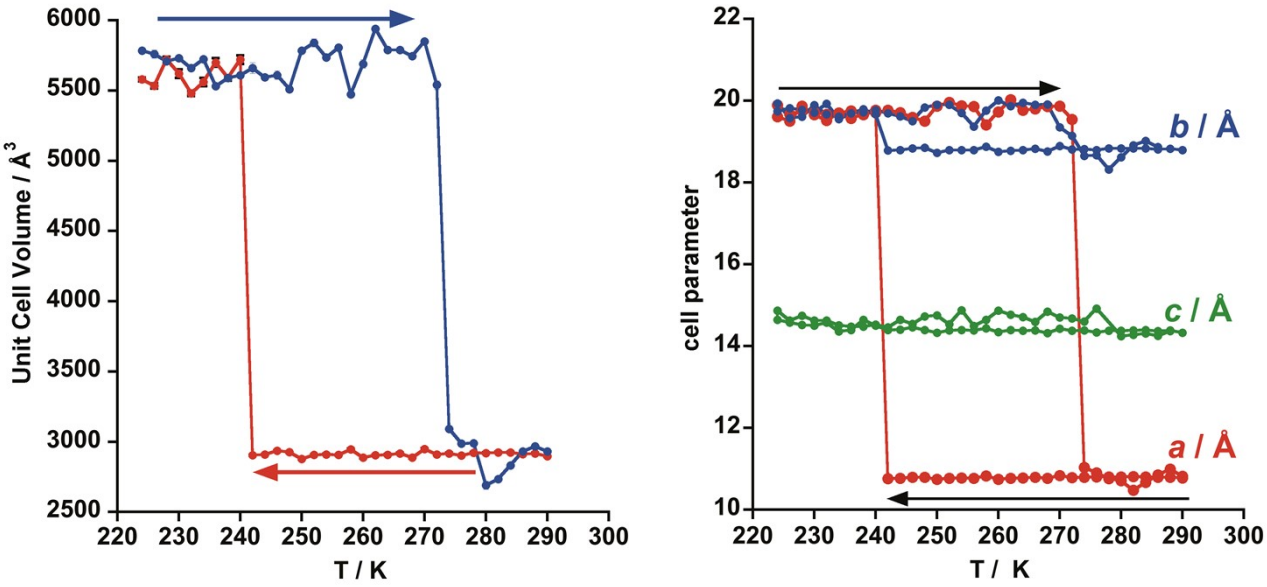

Figure S7. Thermal variation of the crystal parameters *a*, *b*, *c* and of the unit cell volume *V* for **1-BF$_4$**.

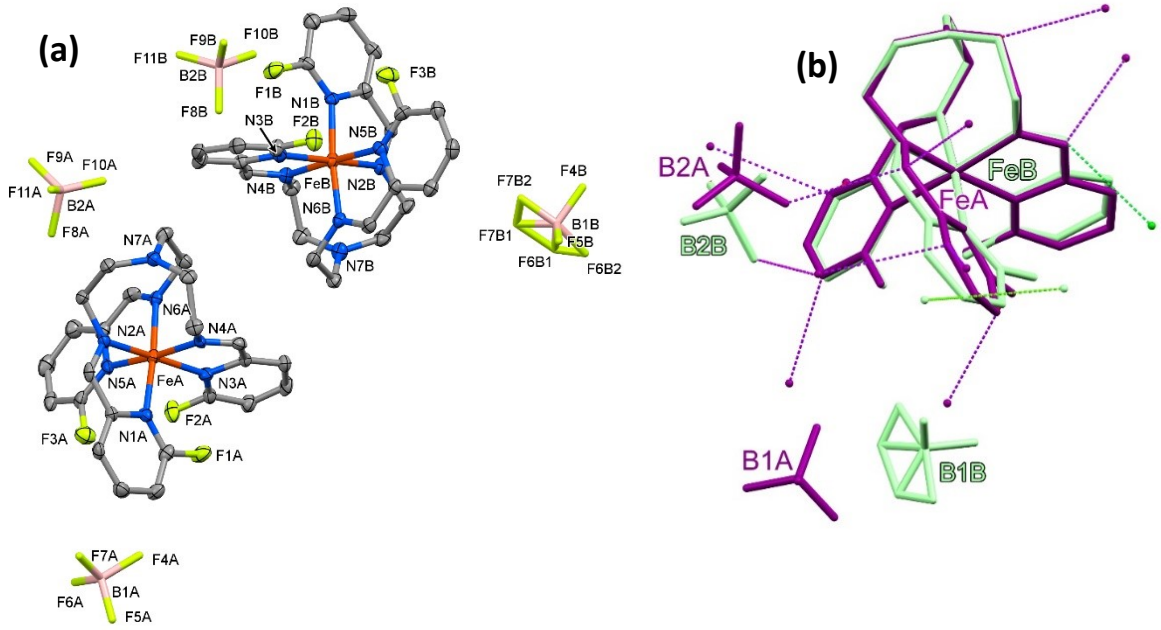

Figure S8. (a) Projection of the complex cations and anions of **1-BF$_4$** at 180 K and (b) their minimized overlay with the closest interactions below the van der Waals radii drawn as dashed lines. The interactions correlate with the complex cations by colour.

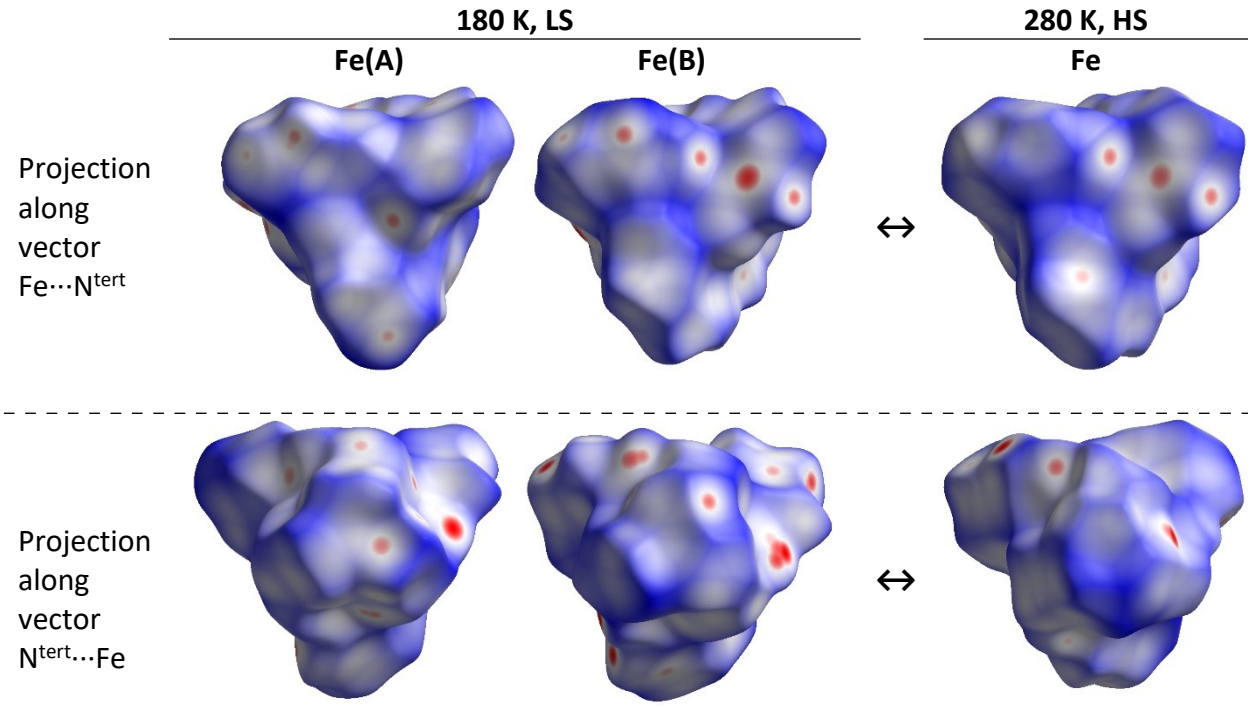

Figure S9. Projection of mapped Hirshfield surface of the left-handed complex cation of **1-BF$_4$** at 280 K and two independent cations at 180 K. The scale of the surface corresponds to the intermolecular contacts with the distances longer (blue), equal (white) or shorter (red) than the van der Waals radii.

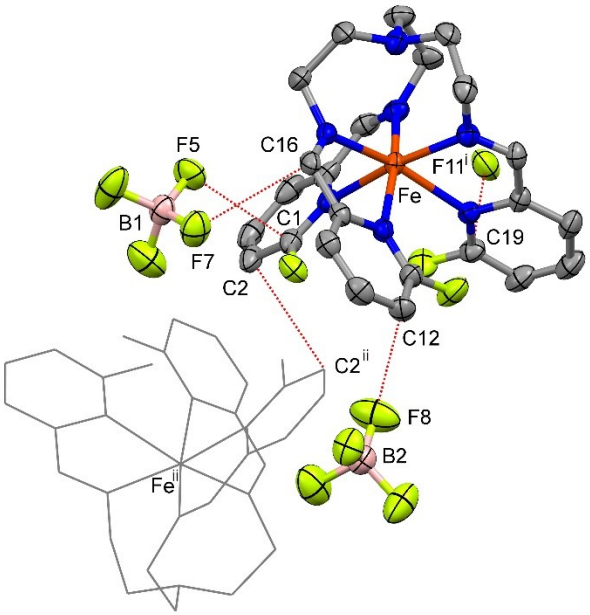

Figure S10. Contacts C···C and C···F below the van der Waals radii drawn of **1-BF$_4$** at 280 K between neighbour complex cations and anions. Symmetry codes: (i) 1 – *x*, 1/2 + *y*, 1.5 – *z*; (ii) 1 – *x*, 1 – *y*, 1 – *z*.

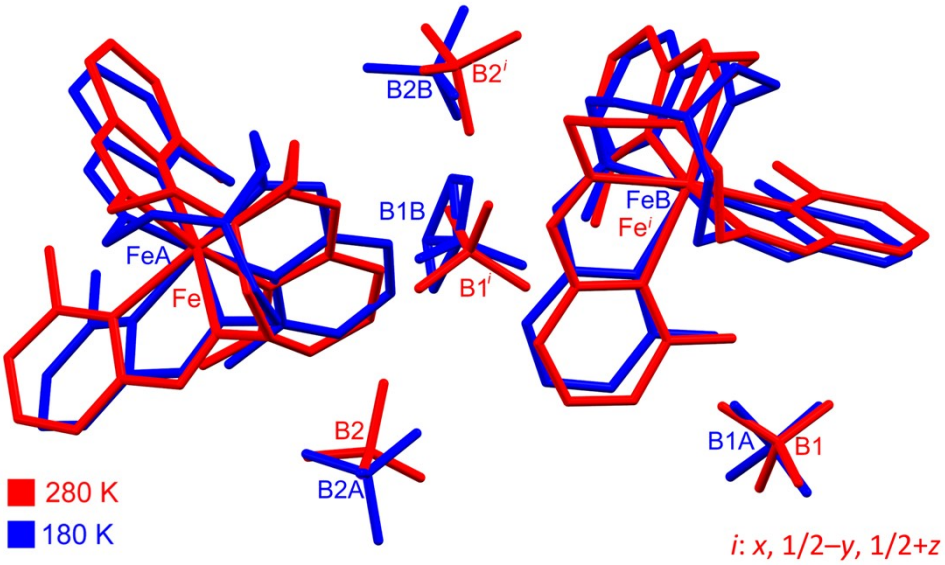

Figure S11. Minimized overlay of the LS and HS structures of **1-BF$_4$**.

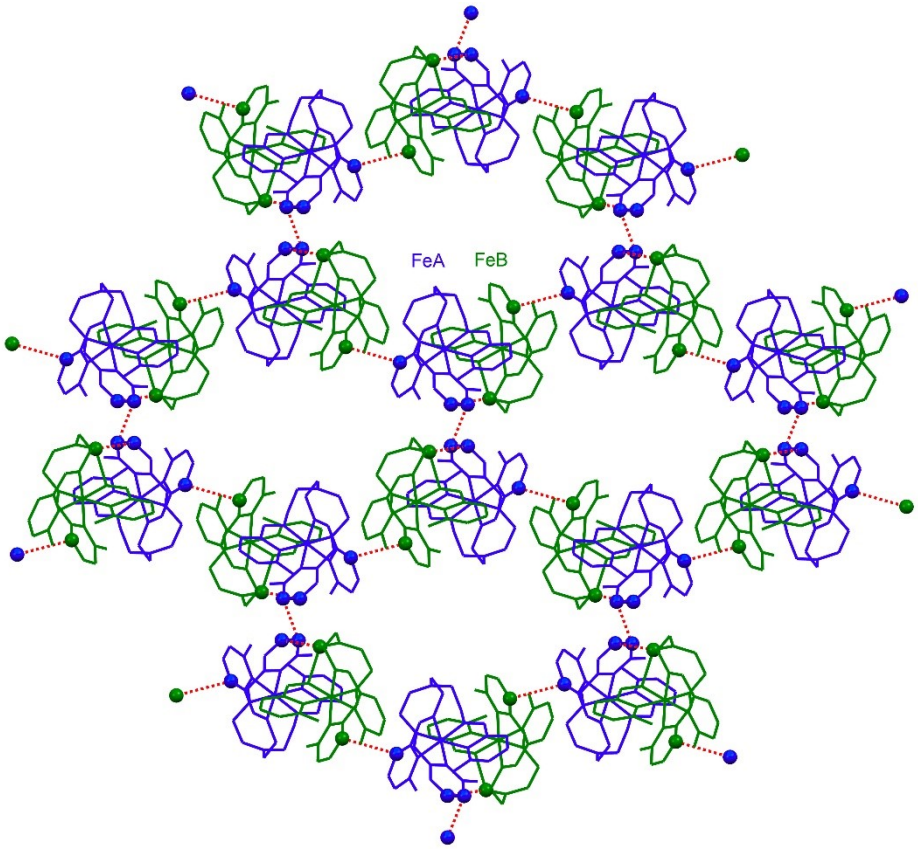

Figure S12. Supramolecular network of **1-BF$_4$** formed by short contacts C···C (red dashed lines) between complex cations at 180 K.

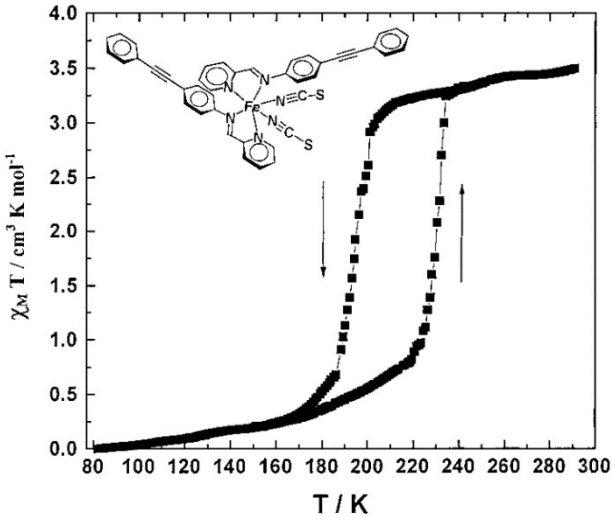

JACS **1997**, 10861

http://doi.org/10.1021/ja972441x

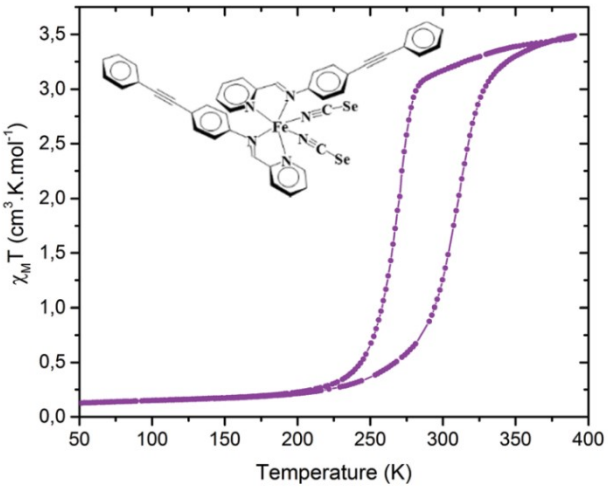

ChemComm **2017**, 4763

http://doi.org/10.1039/c7cc01806a

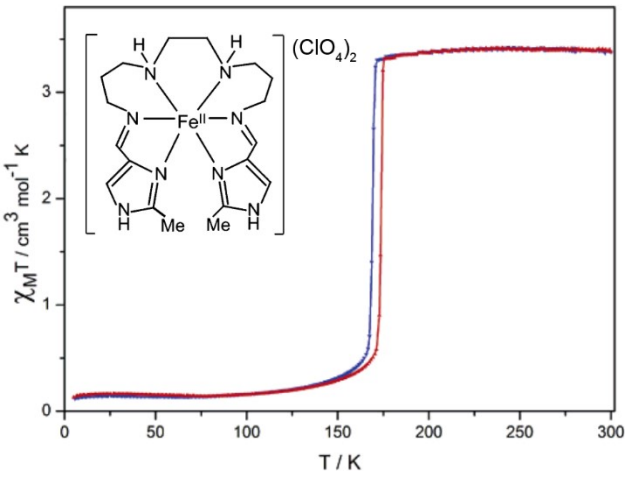

InorgChem **2006**, 8126

http://doi.org/10.1021/ic060674w

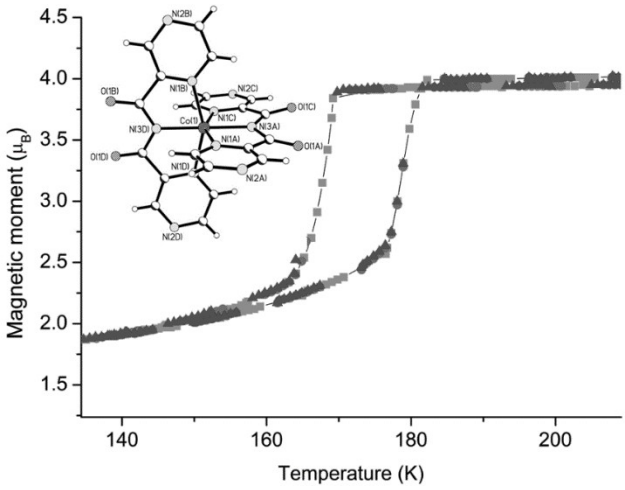

JACS **2012**, 2892

http://doi.org/10.1021/ja208429u

Figure S13. Magnetic curves of several complexes demonstrating onset of gradual ST before an abrupt symmetry-breaking assisted hysteretic ST.

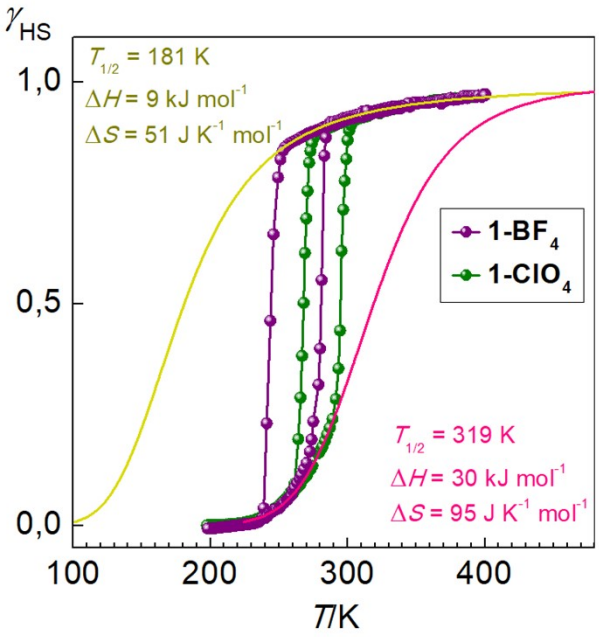

Figure S14. Low- and high-temperature parts of the magnetic curves of **1-BF_4** and **1-ClO_4** simulated by the Slichter-Drickamer model.

REFERENCES

1. G. Sheldrick, Crystal structure refinement with SHELXL, *Acta Crystallogr. Sect. C*, 2015, **71**, 3-8.
2. https://octadist.github.io
3. A. Alousy, J. Burgess and D. L. Elvidge, Solvation of iron(II) complexes of hexadentate tris-diimine Schiff base tripod ligands in alcohol–water and DMSO–water mixtures, *Transit. Met. Chem.*, 2005, **30**, 156-162.
4. M. Seredyuk, A. B. Gaspar, J. Kusz, G. Bednarek and P. Gütlich, Variable-temperature X-ray crystal structure determinations of {Fe[tren(6-Mepy)$_3$]}(ClO$_4$)$_2$ and {Zn[tren(6-Mepy)$_3$]}(ClO$_4$)$_2$ compounds: correlation of the structural data with magnetic and Mössbauer spectroscopy data, *J. Appl. Crystallogr.*, 2007, **40**, 1135-1145.
5. H. R. Chang, J. K. McCusker, H. Toftlund, S. R. Wilson, A. X. Trautwein, H. Winkler and D. N. Hendrickson, [Tetrakis(2-pyridylmethyl)ethylenediamine]iron(II) perchlorate, the first rapidly interconverting ferrous spin-crossover complex, *J. Am. Chem. Soc.*, 1990, **112**, 6814-6827.
6. M. G. B. Drew, C. J. Harding, V. McKee, G. G. Morgan and J. Nelson, Geometric control of manganese redox state, *J. Chem. Soc., Chem. Commun.*, 1995, 1035-1038.
7. M. Buron-Le Cointe, J. Hébert, C. Baldé, N. Moisan, L. Toupet, P. Guionneau, J. F. Létard, E. Freysz, H. Cailleau and E. Collet, Intermolecular control of thermoswitching and photoswitching phenomena in two spin-crossover polymorphs, *Phys. Rev. B*, 2012, **85**.
8. L. J. Kershaw Cook, R. Mohammed, G. Sherborne, T. D. Roberts, S. Alvarez and M. A. Halcrow, Spin state behavior of iron(II)/dipyrazolylpyridine complexes. New insights from crystallographic and solution measurements, *Coord. Chem. Rev.*, 2015, **289**, 2-12.